RSC Advances

PAPER

View Article Online
View Journal | View Issue

Cite this: *RSC Adv.*, 2021, **11**, 21145

Spontaneous alloying of ultrasmall non-stoichiometric Ag–In–S and Cu–In–S quantum dots in aqueous colloidal solutions†

Oleksandr Stroyuk,[a]* Oleksandra Raievska,[bcd] Dmytro Solonenko,[cd] Christian Kupfer,[e] Andres Osvet,[e] Miroslaw Batentschuk,[e] Christoph J. Brabec[ae] and Dietrich R. T. Zahn[cd]

Received 23rd April 2021
Accepted 9th June 2021

DOI: 10.1039/d1ra03179a

rsc.li/rsc-advances

The effect of spontaneous alloying of non-stoichiometric aqueous Ag–In–S (AIS) and Cu–In–S (CIS) quantum dots (QDs) stabilized by surface glutathione (GSH) complexes was observed spectroscopically due to the phenomenon of band bowing typical for the solid–solution Cu(Ag)–In–S (CAIS) QDs. The alloying was found to occur even at room temperature and can be accelerated by a thermal treatment of colloidal mixtures at around 90 °C with no appreciable differences in the average size observed between alloyed and original individual QDs. An equilibrium between QDs and molecular and clustered metal–GSH complexes, which can serve as "building material" for the new mixed CAIS QDs, during the spontaneous alloying is assumed to be responsible for this behavior of GSH-capped ternary QDs. The alloying effect is expected to be of a general character for different In-based ternary chalcogenides.

Introduction

Multinary indium-based ternary and quaternary quantum dots (QDs), such as Cu–In–S (Zn–Cu–In–S) and Ag–In–S (Zn–Ag–In–S), stabilized in aqueous solutions by various multifunctional ligands reveal unique properties stemming from special features of their structure and stabilization mechanism.[1,2] By using bifunctional (such as thioglycolic[3–6] or mercaptopropionic acids), tri-functional (cysteine or glutathione[7–9]), or polyfunctional (*e.g.* polyethyleneimine[10]) ligands, stable colloidal Ag–In–S (AIS) and Cu–In–S (CIS) QDs can be produced in aqueous solutions under mild conditions by means of "green" colloidal chemistry with a variety of compositions and sizes, showing high potential for applications in light-emitting[4,7] and light-harvesting[5,9] applications. The multifunctional ligands saturate under-coordinated metal atoms on the QD surface *via* coordination bonds and, at the same time, form an electrostatic barrier precluding inter-QD interactions and their agglomeration.[1,2] In direct aqueous synthesis with multifunctional ligands, they form complexes with Ag^{I} (Cu^{I}), Zn^{II}, and In^{III} cations, which then act as "building blocks" of the forming QDs and, simultaneously, as stabilizing agents adsorbed on the QD surface. In this way, the surface of colloidal ternary QDs remains at a constant equilibrium with the molecular complexes, which can reversibly adsorb on and desorb from the QD surface. In the exemplary case of GSH-capped AIS QDs, the labile character of surface passivation results in unique temperature-dependent photoluminescence (PL) properties, specifically, in a reversible PL quenching by water due to the thermally activated dissociation/restoration of metal–GSH complexes on the QD surface.[11]

Here we report on an new effect of spontaneous alloying of aqueous GSH-stabilized CIS and AIS QDs into solid–solution Cu(Ag)–In–S (CAIS) QDs. The effect can be observed by absorption and PL spectroscopy and becomes possible due to labile equilibria between the surface of very small CIS and AIS QDs (about 2 nm) and Cu–GSH (Ag–GSH) complexes serving as capping ligands. The alloyed CAIS QDs reveal a lower bandgap as compared to the original CIS and AIS QDs indicating a higher thermodynamic stability of mixed QDs. This factor shifts the QD-complex equilibria toward the formation of mixed CAIS QDs and provides a driving force for the spontaneous alloying of CIS and AIS QDs. Such phenomena have not been reported before

[a]*Forschungszentrum Jülich GmbH, Helmholtz-Institut Erlangen Nürnberg für Erneuerbare Energien (HI ERN), Erlangen 91058, Germany. E-mail: o.stroyuk@fz-juelich.de*

[b]*L. V. Pysarzhevsky Institute of Physical Chemistry, Nat. Acad. of Science of Ukraine, Kyiv 03028, Ukraine*

[c]*Semiconductor Physics, Chemnitz University of Technology, Chemnitz D-09107, Germany*

[d]*Center for Materials, Architectures, and Integration of Nanomembranes (MAIN), Chemnitz University of Technology, Chemnitz D-09107, Germany*

[e]*Friedrich-Alexander-Universität Erlangen-Nürnberg, Materials for Electronics and Energy Technology (i-MEET), Martensstrasse 7, Erlangen 91058, Germany*

† Electronic supplementary information (ESI) available: Tabulated data on the XRD reflections of tested QDs and spectral PL characteristics of CIS + AIS QDs systems aged at 25 and 96–98 °C; representative AFM images and size distributions for original and thermally treated CIS, AIS, CAIS QDs, and CIS + AIS QD systems; PL maximum energies of CIS + AIS and CISe + AISe QD systems aged at room temperature at different copper-to-silver ratios; details of the syntheses of colloidal CIS and AIS QDs. See DOI: 10.1039/d1ra03179a

for the ternary In-based QDs and can open new venues for highly controlled combinatorial syntheses of more complex multinary QDs from simpler QD "building blocks".

Experimental

Materials

$InCl_3$, $AgNO_3$, $Cu(NO_3)_2 \times 3H_2O$, reduced GSH, aqueous 5.0 M NH_4OH solution, 69 w% HNO_3, citric acid, $Na_2S \times 9H_2O$, and 2-propanol were supplied by Merk and used without additional purification. Deionised (DI) water was used in all experiments.

Synthesis of colloidal QDs

Aqueous colloidal AIS, CIS, and CAIS QDs capped with surface GSH complexes were produced according to previously reported protocols[7–9] *via* interaction between GSH complexes of Ag^I (or Cu^{II} or a mixture of Ag^I and Cu^{II}) and In^{III} with Na_2S in alkaline solutions followed by a thermal treatment at 96–98 °C for 180 min. The nominal molar ratio of Ag^I (or Cu^{II} or $Cu^{II} + Ag^I$) to In^{III} was set at 1 : 4. In a typical procedure, to 2.4 mL DI water 0.8 mL aqueous 1.0 M $InCl_3$ solution (with 0.25 M HNO_3 to avoid In^{III} hydrolysis), 2.4 mL aqueous 0.5 M GSH solution, 1.0 mL aqueous 5.0 M NH_4OH, 0.1 mL aqueous 2.0 M solution of citric acid, and 2.0 mL aqueous 0.1 M solution of $AgNO_3$ (for AIS QDs), $Cu(NO_3)_2$ (for CIS QDs), or a mixture of 1.0 mL aqueous 0.1 M $AgNO_3$ and 1.0 mL aqueous 0.1 M $Cu(NO_3)_2$ (for CAIS QDs) were added consecutively under intense stirring followed by 1.0 mL of aqueous 1.0 M solution of Na_2S. The as-prepared solutions were transferred to cylindric vials 1.0 cm in diameter and subjected to heating at 96–98 °C without reflux in a boiling water bath for 3 h. After heating DI water was added to each solution to restore the original volume (10 mL).

Instruments

Absorption and PL properties of colloidal solutions were registered in standard 10.0 mm quartz optical cuvettes using a Black Comet CXR-SR UV/Vis/NIR spectrometer (StellarNet Inc., USA) equipped with miniature deuterium/halogen lamps (absorption spectra) or a 390 nm diode (PL spectra) as an excitation source and 100 μm slits in the range of 220–1100 nm. Colloidal solutions were diluted prior to the measurements (0.001 mL per 2.5 mL DI water). Absorption spectra were acquired for an accumulation time of 100 ms with five consecutively taken spectra averaged and the absorbance of a cuvette with pure DI water substracted from the final spectrum. PL spectra were registered with an acquisition time of 500 ms and normalized to the absorbance of the colloids at 390 nm. PL excitation spectra were registered for diluted colloidal QD solutions using a Jasco FP-8500 luminescence spectrometer at the PL band maximum of each measured colloidal solution. PL quantum yields were evaluated using previously reported aqueous colloidal AIS/ZnS QDs as a PL standard with a PLQY of 50%.[7]

The kinetic curves of PL decay of colloidal solutions were registered using a FluoTime300 luminescence spectrometer (PicoQuant) equipped with 402 nm LDH-P-C-405B laser collecting the PL signal in the range of 450–800 nm. The samples (200 μL) were placed in the pits of a standard Eppendorf palette and excited from the pit tops (4–5 mm above the surface). The average PL lifetimes were determined by fitting the PL decay curves with linear combinations of three monoexponential functions with amplitudes and time constants of separate components set as fitting parameters.[7,11]

X-ray diffractograms were collected using a Rigaku SmartLab diffractometer in an angle range of $2\theta = 5°$–$100°$ with a step rate of 0.05° per min using 9 kV copper Kα irradiation. The samples were produced by drop-casting QD colloids on a glass plate at room temperature. The drop-cast solutions were dried in vacuum. Equal amounts of the various colloidal samples were deposited on the glass plates to enable comparison of the peak intensities.

AFM images were acquired with an AFM 5500 from Keysight (Agilent). The AFM tip had a radius of 10 nm and the Si cantilever a resonance frequency of 180 kHz. The samples were prepared by drop-casting of a very diluted (to the order of 10^{-5} M in terms of Ag (Cu) concentration) colloids on a freshly cleaved mica surface and dried in a nitrogen stream at room temperature. No ultrasound treatment of the colloidal samples was performed. The original concentrated QD samples were diluted, drop-casted on mica, and measured by AFM within 5–10 min after the event of dilution to minimize possible deterioration of the samples. The QD size distribution charts were plotted based on AFM measurements of the height profiles for several hundred separate QDs. The AFM images were processed using the Gwyddion software (with "plane substraction" and "aligning rows" filters, and zero leveling) and marked by using the edge-detection grain marking tool of Gwyddion and the distributions of mean height were plotted for each image. The QD volume-weighted distributions were derived from original numerical distributions by multiplying the QD count on the QD volume for each particular size.

Results and discussion

By following our recent report on CAIS QDs[9] we probed the stationary and time-resolved PL behavior of these solid solution QDs comparing it to the behavior of mechanical mixtures of separately synthesized GSH-capped CIS and AIS QDs with the same copper-to-silver ratios. In these experiments we found that the spectral properties of the CIS + AIS QD mixtures (positions of the absorption and PL bands, PL life time, *etc.*) change gradually at room temperature. This evolution becomes much faster at elevated temperatures. To gain deeper insights into the dynamics and possible origins of such spectral changes we focused on colloidal mixtures of CIS and AIS QDs with a nominal molar ratio of $[Cu^+] : [Ag^+] = 1 : 1$ tracking the temporal evolution of their spectral characteristics at 25 °C and 96–98 °C (in colloidal solutions kept in a boiling water bath).

The spectral changes in mixtures of AIS and CIS QDs observed during the thermal treatment at 96–98 °C and resulting from inter-QD interactions can be complicated by processes of Ostwald ripening of individual QDs and, possibly, their surface oxidation. To distinguish between the inherent thermally-activated changes of the optical properties of AIS, CIS,

and CAIS QDs from those resulting from the alloying between CIS and AIS we tracked the positions and shapes of absorption, PL, and PL excitation (PLE) bands separately for each individual composition simultaneously with CIS + AIS mixtures. All QD samples studied reveal bandgaps much higher than their bulk counterparts,[2] indicating effects of spatial exciton confinement and allowing possible changes in the size/size distribution of AIS, CIS, and CAIS QDs to be tracked by observing changes in the positions of their absorption, PL, and PLE bands.

The GSH-capped AIS QDs reveal broad absorption bands with an edge at around 2 eV that can be determined more precisely by presenting the spectra in the Tauc coordinates and plotting a tangent to the linear sections of the spectra till the zero ordinate. In this way, the bandgap of AIS QDs was found at 2.16 eV, shifting to 2.12 eV as a result of the ageing at 96–98 °C for 60 min (Fig. 1a, curves 1a and 2a). The small "red" shift of the absorption edge indicates a limited evolution of the average size and size distribution in the ensemble of AIS QDs. In a similar way, the PL band maximum shifts upon thermal treatment by merely 20 meV, from 2.06 to 2.04 eV (Fig. 1a, curves 1b and 2b). The same small shift of 20 meV is observed in the PLE spectra of AIS QDs (compare corresponding curves in Fig. 1f and g), indicating insignificant changes in the optical properties of the AIS QD ensemble upon thermal ageing. The PL QY of AIS QDs was found to be almost constant changing from 30% before the thermal treatment to 31% after the heating.

Qualitatively the same situation is observed for GSH-capped colloidal CIS QDs (Fig. 1b). In this case, the thermal treatment also results in small "red" shifts of the absorption, PLE band edges, and PL band maximum, respectively, from 1.93 to 1.89 eV (absorption), from 1.98 to 1.93 eV (PL), and from 1.97 to 1.95 eV (PLE) with no appreciable changes in the band shapes. The PL QY of CIS QDs was found to be 3% both before and after the thermal treatment.

The solid–solution CAIS QDs (Fig. 1c) show similar small changes of the positions of the absorption and PLE band edges and PL band maximum, shifting from 1.88 to 1.81 eV (absorption), from 1.91 eV to 1.86 eV (PL), and from 1.85 to 1.83 eV (PLE). For such solid–solution QDs the absorption edge can be found at much lower energies as compared to individual AIS and CIS QDs due to the effect of band bowing discussed in detail in our previous report.[9] The positions of PLE band edge and PL band maximum of CAIS QDs are also subject to the band bowing effect showing lower values as compared to both individual compounds.

Fig. 1e shows normalized PL spectra of AIS, CIS, and CAIS QDs after the thermal treatment showing clearly the "red" shift of the PL band of the solid–solution CAIS QDs relative to AIS and CIS QDs. The nature of the band bowing effect is still under discussion. A lattice disordering and local fluctuations of the composition are among the most frequently argued reasons for

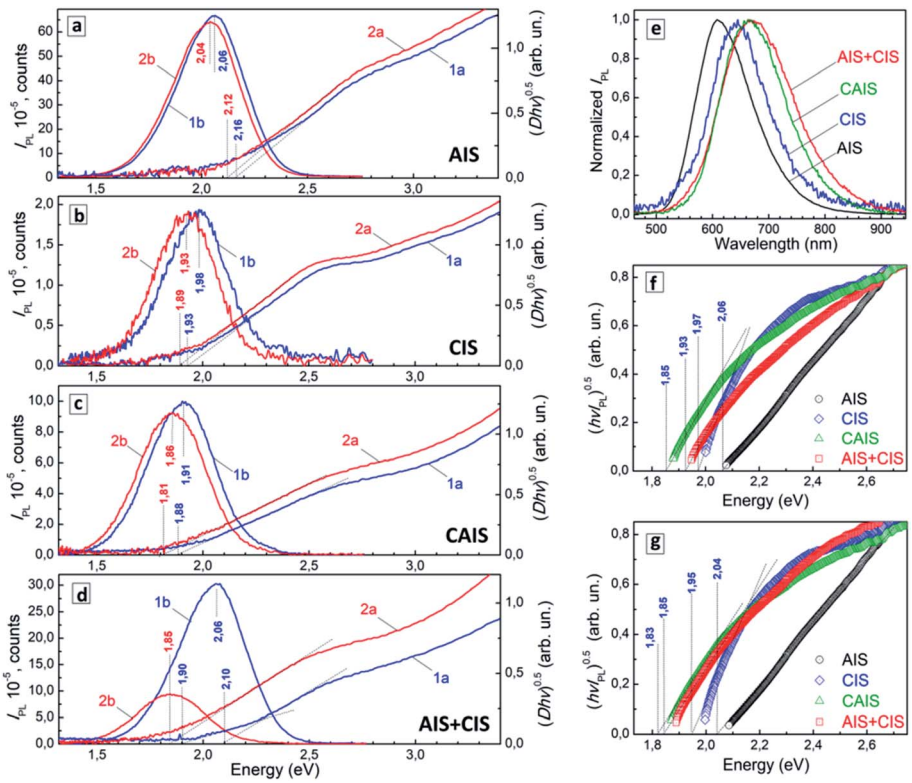

Fig. 1 (a–d) Absorption (curves a) and PL spectra (curves b) of colloidal AIS QDs (a), CIS QDs (b), mixed CAIS QDs (c) and a 1 : 1 mixture of AIS and CIS QDs (d) directly after the mixing of QDs (curves 1) and after thermal treatment at 96–98 °C for 60 min (curves 2). (e) Normalized PL spectra of thermally treated AIS, CIS, CAIS QDs as well as the CIS + AIS mixture. (f and g) PL excitation spectra of AIS, CIS, CAIS, and CIS + AIS before (f) and after the thermal treatment at 96–98 °C for 60 min (g) presented in the coordinates of the Tauc equation.

the band bowing of intermediate Cu–Ag–In–S compounds as compared to pure AIS and CIS of the same Ag(Cu)-to-In ratio.

Surprisingly, a mixture (1 : 1 in terms of moles of M^I species, M = Ag, Cu) of individual CIS and AIS QDs subjected to the thermal treatment at 96–98 °C showed the strongest spectral changes that have no analogs in the cases of CIS, AIS, and CAIS QDs. In particular, the absorption edge of the QD mixture was shifted upon heating by 200 meV, from 2.10 to 1.90 eV (Fig. 1d, curves 1a and 2a), that is, 5 times stronger than for AIS and CIS QDs. The PL band maximum shows the same strong shift from 2.06 to 1.85 eV (Fig. 1d, curves 1b and 2b).

The final position of the PL band maximum of the thermally treated CIS + AIS mixture has a lower energy as compared to both AIS and CIS QDs and approaches that of the thermally treated CAIS QDs (Fig. 1e) with both CAIS and CIS + AIS colloids having formally the same chemical composition but totally different preparation history. The PL QY of the CIS + AIS mixture was found to lower from 16% before the thermal treatment to 7% after the heating.

The PLE spectra additionally show the vivid evolution of the PL properties of the CIS + AIS mixture (Fig. 1f and g). Before the thermal treatment the CIS + AIS shows a PLE edge energy intermediate between AIS and CIS which is expected for a mixture, but already shifted more to the value typical for CIS QDs. After the thermal treatment, the CIS + AIS QD mixture reveals a PLE edge energy (1.85 eV) lower than both CIS QDs (1.95 eV) and AIS QDs (2.04 eV) and very close to that of solid–solution CAIS QDs (1.83 eV).

Based on the discussed spectral observations we can conclude that the thermal treatment of a mixture of CIS and AIS QDs results in their gradual transformation into mixed solid–solution QDs showing almost the same spectral properties as thermally-treated solid–solution CAIS QDs produced originally from a mixture of Ag^I and Cu^{II} complexes with GSH. These spectral transformations are specific only for the case of the CIS + AIS QD mixture and are not observed for individual CIS and AIS QDs as well as for the solid–solution CAIS QDs subjected to the same treatment indicating that a chemical transformation takes place in the mixed CIS + AIS colloidal solution.

Additionally to the spectral studies we characterized the thermally-treated CIS, AIS, CAIS, and CIS + AIS QDs with X-ray diffraction (XRD) and atomic force microscopy (AFM). The XRD patterns of all QDs have the same structure (Fig. 2a) exhibiting three major strongly broadened peaks corresponding to (112), (220), and (312) planes typical for a chalcopyrite lattice, with the solid–solution CAIS QDs having intermediary peak positions between those of CIS and AIS (see Table S1 in ESI†) in agreement with our previous report.[9] Probing the valence state of copper in CIS QDs with X-ray photoelectron spectroscopy (ESI, Fig. S1† and related discussion) revealed it to be present as Cu^I with no detectable signs of Cu^{II} species, in accordance with the expected chalcopyrite structure.

As the XRD patterns do not allow distinguishing between the mixtures of QDs and the solid–solution QDs of the same nominal composition due to the very broadened character of reflections we can only conclude from the presented data that no new phases are formed as a result of the thermal treatment of the CIS + AIS QD mixture. Therefore, we cannot assign the spectral changes observed to some phase transformations occurring in the mixture.

The average size of all studied QDs as well as that of the thermally treated CIS + AIS QD mixture estimated from the XRD reflection broadening was found to be about 2 nm irrespective of the QD composition (ESI, Table S1†). The latter observation indicates that we cannot assign the spectral changes in the CIS + AIS QD mixture to significant variations of the average QD size.

The latter conclusion is supported by AFM-based estimations of the size distributions in the studied colloidal systems. The QDs were dispersed on atomically flat mica allowing the height (that is the size) of many hundreds of separate QDs to be measured from each image. By analyzing the QD volume-weighted size distributions we found no noticeable thermally-induced changes of the average size in the case of AIS QDs (ESI, Fig. S1†) as well as an increase of the average size from 1.4 nm to 1.8 nm for CIS QDs (ESI, Fig. S2†) and from 1.6 nm to 1.8 nm – for CAIS QDs (ESI, Fig. S3†), which is in accordance with the spectral observations. In a similar way, the mixture of CIS and AIS QDs showed a very small change of the average size from about 1.6 nm to 1.7 nm as a result of the thermal treatment (ESI, Fig. S4†).

Fig. 2b provides a comparative illustration of the QD volume-weighted size distributions for all studied samples after the thermal ageing. We see that the size distribution in the CIS + AIS QD mixture is roughly the same as for the solid-state CAIS QDs originally produced from a mixture of Ag^I and Cu^{II} complexes with GSH. These data, along with the XRD-based estimations, show that the strong spectral changes observed during the thermal treatment of the CIS + AIS QD mixture cannot be explained by changes in the average QD size or some sort of QD agglomeration.

Thus, by excluding the size evolution, the QD agglomeration, and the formation of new phases as possible reasons for the spectral changes in the mixed CIS + AIS QD system we can take the spontaneous alloying between CIS and AIS into CAIS QDs as the most probable reason for the spectral evolutions observed during the thermal treatment of the QD mixtures.

Additional arguments for this conclusion were supplied by time-resolved PL spectroscopy. Fig. 3a illustrates normalized kinetic curves of PL decay for the AIS, CIS, and CAIS QD colloids

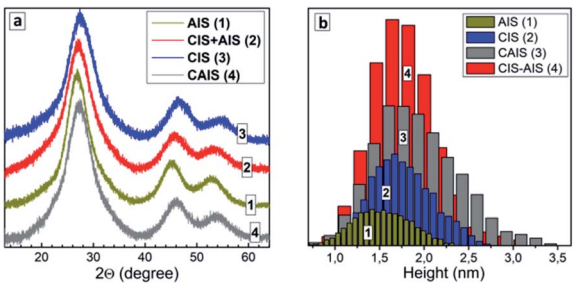

Fig. 2 XRD patterns (a) and size distributions derived from AFM images (b) for AIS, CIS, and CAIS QDs as well as for AIS–CIS mixture aged at 96–98 °C for 60 min.

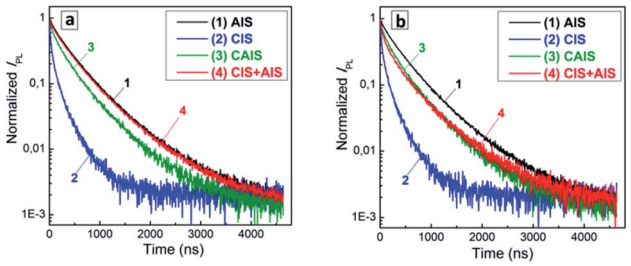

Fig. 3 Kinetic curves of PL decay registered in the PL band maxima for AIS QDs (curves 1), CIS QDs (2), CAIS QDs (3), and 1 : 1 mixtures of AIS and CIS QDs (4) kept for 60 min at 25 °C (a) and 96–98 °C (b).

Table 1 Average PL lifetime (ns) for different individual QDs and QD compositions

	AIS	CIS	CAIS	CIS + AIS
No heat treatment	480	160	395	470
Heating at 96–98 °C	485	160	400	415

as well as for the 1 : 1 mixture of CIS and AIS QDs before any thermal treatment. The AIS QDs showed the slowest PL decay with an average PL lifetime τ_{PL} of 480 ns (Table 1). The CIS QDs revealed a distinctly faster PL decay with τ_{PL} of 160 ns, while the solid–solution CAIS QDs showed τ_{PL} = 395 ns intermediate between AIS and CIS QD samples. As the PL intensity of AIS QDs is roughly by two orders of magnitude higher than that for CIS QDs (compare PL spectra in Fig. 1a and b), the PL decay curve of the 1 : 1 mixture of CIS and AIS QDs almost coincided with that of pure AIS QDs, the latter having the dominant contribution to the PL signal.

The thermal ageing of AIS, CIS, and CAIS QDs was found to have a very small effect on the PL decay behavior (compare Fig. 3a and b) with the average PL lifetime changing insignificantly for AIS and CAIS and not changing at all for CIS QDs (Table 1). On the contrary, the PL decay curve of the thermally-treated 1 : 1 CIS + AIS QD mixture showed a pronounced evolution toward the PL decay curve of CAIS QDs (compare curves 3 and 4, Fig. 3b). The average PL lifetime of the mixture is lowered from 470 ns to 415 ns (Table 1), which is close to τ_{PL} of the solid–solution CAIS QDs.

This strong τ_{PL} change of the CIS + AIS mixture along with almost unchanged PL decay parameters of individual CIS, AIS, and solid–solution CAIS QDs is a clear indication of chemical transformations taking place in the CIS + AIS QD system.

To gain more insights into the transformations observed in the CIS + AIS QD mixtures we followed the temporal evolution of the spectral PL properties for two different temperatures, namely 25 °C and 96–98 °C, inspecting both concentrated and strongly diluted (by a factor of 1000) 1 : 1 CIS + AIS mixtures for each temperature in the dark (to eliminate possible photoinduced processes). Distinct changes in the PL band position can be observed both for concentrated and diluted solutions even at room temperature (Fig. 4a, curves 1 and 2). In particular, the PL band maximum energy was found to decrease by 40–50 meV during the six-hour observation both for concentrated and diluted 1 : 1 CIS + AIS QD mixtures (Fig. 4c, 1 and 2). Simultaneously, the PL intensity was found to decrease almost by 50% during this period, while the spectral width of the PL band (w_{PL}) shows a distinct increase (ESI, Tables S2 and S3†). These spectral changes indicate that the spontaneous alloying slowly occurs in the mixed solution at room temperature.

At the same time, a "red" spectral shift of the PL band becomes clearly observable at 96–98 °C already within tens of minutes of the thermal ageing both in the concentrated and diluted systems (Fig. 4b). The shift of the PL band energy was found to evolve at elevated temperature faster in the concentrated CIS + AIS solution than in the diluted one (Fig. 4c, 3 and 4). After a 20 min thermal treatment of the colloidal solution the PL energy maximum shows a decrease of around 200 meV, while the original PL intensity is reduced by a factor of 5 (ESI, Table S4†). The w_{PL} shows a tiny decrease that can be associated with the Ostwald ripening and a narrowing of the QD size distribution simultaneous to the spontaneous CIS + AIS alloying. The same but slower evolution of the spectral PL parameters was observed for the diluted CIS + AIS QD mixtures kept at 96–98 °C (ESI, Table S5†).

The effect of spontaneous alloying of mixed CIS and AIS QDs can be interpreted in terms of the existence of an equilibrium

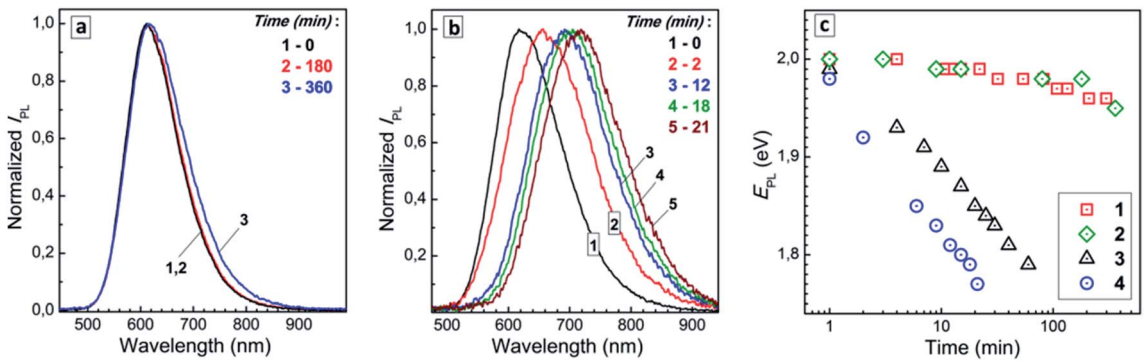

Fig. 4 Normalized PL spectra of a concentrated 1 : 1 mixture of colloidal AIS and CIS QDs kept at 25 °C (a) and 96–98 °C (b). (c) Evolution of PL band maximum energy (E_{PL}) for diluted (1 and 3) and concentrated (2 and 4) mixtures of colloidal AIS and CIS QDs kept at 25 °C (1 and 2) and 96–98 °C (3 and 4).

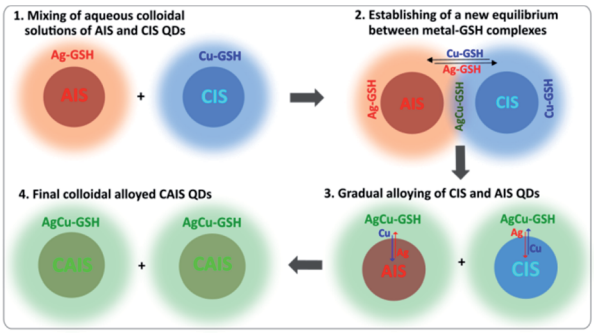

Fig. 5 A scheme illustrating spontaneous alloying of CIS and AIS QDs induced by metal–complex equilibria on the QD surface.

between the QDs capped with metal–GSH complexes and dissolved molecular forms of such complexes as well as various cluster-like species intermediary between molecular complexes and QDs (Fig. 5). Such species are always present in the colloidal systems studied and can be clearly observed in AFM images.

The numerical size distributions obtained for the colloidal solutions before the thermal treatment always show a fraction of species smaller than 0.6–0.8 nm (ESI, Fig. S2–S5,† curves 1), which can be assigned to such molecular and clustered metal–GSH complexes serving both as building blocks and as capping ligands for the QDs. Such capping ligands reside in an equilibrium between the QD surface and the dispersive medium, which can be shifted by thermal activation resulting, for example, in peculiar temperature dependences of PL properties of AIS QDs reported by us earlier.[11,12] As the colloids are subjected to the thermal treatment, the population of such species is strongly decreased due to the redistribution in Ostwald ripening-like processes.

We may, therefore, assume that when two colloidal systems – AIS QDs and CIS QDs – are brought into contact, a new equilibrium should establish corresponding to the energy minimum for the newly formed system (Fig. 5). The band bowing effect observed in CAIS QDs, that is, the narrowing of the bandgap of the solid–solution QDs as compared to individual components, is a clear indication that the mixed CAIS QDs have a lower interband electron transition energy and therefore should be thermodynamically more stable than separate CIS and AIS QDs. This fact favours a gradual formation of mixed CAIS QDs from the molecular "building blocks" present in both AIS and CIS QD solutions. At that, the equilibrium between QDs and molecular metal–GSH complexes or, quite probably, some ultra-small and stable "magic-size" clusters would shift toward the latters and the original QDs dissolve gradually while supplying the "building material" for the formation of new solid–solution CAIS QDs.

The magic-size clusters intermediary between molecular and solid-state of metal chalcogenide semiconductors are currently recognized as ever-present precursors for the formation of many binary II–VI and IV–VI compounds,[13,14] but such species are still to be discovered and studied for ternary metal–chalcogenide semiconductors, like CIS or AIS. The thermally activated redistribution between such magic-size clusters and QDs, from one side, and molecular species, from the other side, can be strongly facilitated by the presence of multifunctional GSH, which can form covalent bonds with the QD surface, coordination bonds with metal cations, ionic bonds with chalcogenide anions, and serve as a universal "shuttle" among CIS and AIS QD and clusters during the spontaneous alloying.

The phenomena of spontaneous alloying were reported for various binary mixtures of nanometer particles of monoatomic (mostly metallic) species and semiconductor compounds.[15–23] In particular, the spontaneous alloying was observed for mechanical mixtures of alkali metal halide particles as large as 200 nm. The kinetics of this process was governed by the ratio of the ionic radii of both the cationic and anionic components.[15] Iodine was found to alloy spontaneously with 100 nm silver particles to form more stable AgI phases.[16] Spontaneous alloying between Ag and Pd nanoparticles was found to occur at room temperature in aqueous solutions resulting in Ag-diffused Pd particles of the same shape as the original pure Pd nanocrystals.[17] A strong size dependence of the spontaneous alloying between gold cores and silver shells was found for Au core sizes varied from 2.5 to 20 nm.[18] The lattice defects on the surface of Au cores were assumed to be largely responsible for the Au–Ag interdiffusion and alloying and this factor can account for the size dependence, since the defect density is higher for smaller Au cores.[18]

The theoretical calculations performed for Ag and Cu clusters revealed clear dependences of the dynamics of spontaneous alloying between different metal clusters both on the temperature and the cluster size.[19–21] The critical cluster size for the Au–Cu system was around 1 nm[19] with an additional external source of thermal or mechanical energy required to alloy larger formations. Spontaneous alloying between Au and Sb clusters was observed experimentally by *in situ* TEM and found to be strongly enhanced as the cluster size is decreased.[22] The same authors reported the phenomena of spontaneous alloying of 4 nm particles of ZnS and CdSe with the formation of corresponding solid–solution particles,[23] which is of high relevance to the presently reported effects. No alloying was observed for ZnS shells deposited onto larger 6 nm CdSe particles,[23] indicating a critical effect of the particle size for the effect of spontaneous alloying to occur.

Typically, a quasi solid-state mechanism is assumed for the spontaneous alloying of metal and semiconductor nanoparticles without intermediate stages of melting or dissolution[17,22,23] allowing, for example, the shape of the original particles to be conserved.[17] At the same time, the alloying between molecular-like silver $Ag_{25}(SR)_{18}$ and gold $Au_{25}(SR)_{18}$ clusters (SR is a thiol) was assumed to proceed *via* the exchange of gold and silver atoms among the clusters bound together into an experimentally detected $Au_{25}Ag_{25}(SR)_{36}$ adduct.[24] By reacting these atomically precise (in terms of composition) gold and silver clusters in different proportions a series of $Ag_mAu_n(SR)_{18}$ clusters ($m + n = 25$) with an arbitrarily-tailored composition can be produced.[24]

In the light of these reports and our experimental evidence, we can assume that the effects of the spontaneous alloying

observed in the present CIS–AIS system can be accounted for by both the very small QD size, about 1–2 nm, and the equilibrium between QDs and molecular clusters. The latter serve as mass shuttles supplying the material for the formation of new alloyed QDs. We can thus imagine two possible mechanisms of the formation of alloyed CAIS QDs from CIS and AIS QDs. The first one (discussed above) assuming gradual dissolution of the original QDs into molecular cluster species forming new CAIS QDs, while the second one requires a coupling between a CIS QD and an AIS QDs followed by GSH-assisted silver/copper exchange in such adduct similar to the case of the silver–gold cluster adduct reported in ref. 24.

The driving force behind the spontaneous alloying is assumed to be a higher thermodynamic stability of alloyed CAIS QDs evidenced by their lower bandgap as compared to the starting CIS and AIS QDs (the band bowing effect[9]). A similar scenario is realized at the Ostwald ripening of the differently sized metal–chalcogenide QDs. The smaller QDs with a larger bandgap are less stable and more soluble than larger QDs with a lower bandgap resulting in gradual mass redistribution from smaller to larger QDs. In the present case, the contact between CIS and AIS QDs, both being in an equilibrium with corresponding metal–GSH complexes results in the formation of a more stable CAIS compound, thus shifting the original equilibria toward the formation of CAIS QDs and providing a driving force for the spontaneous alloying.

Our preliminary studies evidenced the general character of the effect of spontaneous alloying, which can be observed for different mixtures of CIX and AIX QDs, where X = S or Se, as well as for different ratios between CIX and AIX QD species. We present two examples in ESI,† showing a distinct band bowing effect in the position of the PL band maximum energy for the products of alloying of aqueous CIS and AIS QDs (Fig. S6a†) and aqueous CISe and AISe QDs (Fig. S6b†) taken in different proportions. In this view, the CIX and AIX QDs can be used as precursors for a highly controlled synthesis of new QDs with more complex compositions and stoichiometries by exploiting the effect of spontaneous alloying. The present report is intentionally focused exclusively on the CIS + AIS pair to analyze a simpler case with the same chalcogenide anion in both components, while a deeper and more extended study of alloying of several components will be presented by us in a further contribution. Also, the details of the mechanism of the spontaneous alloying require a deeper insight in future studies. In particular, we plan to probe the PL properties and the composition of partially and completely alloyed CAIS QDs by time-resolved PL and energy-dispersive X-ray analysis both on a single QD level, as well as to perform a dedicated XPS study of the intermediate products of the spontaneous alloying at different temperatures.

Conclusions

Summarizing, we report an effect of spontaneous alloying of non-stoichiometric GSH-stabilized AIS and CIS QDs in aqueous colloidal solutions. This effect can be vividly observed as the transformation of CIS + AIS QD mixtures into solid–solution CAIS QDs is accompanied by shifts of the absorption, PL, and PLE bands to energies lower than the corresponding energies of the original components due to the effect of band-bowing in mixed GSH-capped CAIS QDs[9S].

The spectral shifts are not accompanied by the formation of new phases or significant changes in the size distributions or aggregation effects in the colloidal CIS + AIS ensemble. In this view, the "red" shifts of absorption and PL features, as well as a shortening of the PL lifetime can only be accounted for by the spontaneous alloying of the original QDs. This process occurs already at room temperature and is strongly accelerated by the thermal treatment of aqueous colloids at temperatures close to the boiling point of water.

An equilibrium between QDs and molecular and clustered metal–GSH complexes, which can be used as a "building material" for new mixed CAIS QDs, during the spontaneous alloying is assumed to be responsible for this behavior of GSH-capped ternary QDs, and, therefore, be of a general character for different CIS(Se) and AIS(Se) QDs.

Author contributions

O. Stroyuk and O. Raievska – conceptualization, investigation, methodology, writing – original draft; D. Solonenko – investigation, writing – review & editing; C. Kupfer – investigation, A. Osvet – investigation, methodology; M. Batentschuk – methodology, writing – review & editing, C. J. Brabec – conceptualization, writing – review & editing, funding acquisition; D. R. T. Zahn – conceptualization, writing – review & editing, funding acquisition, project administration.

Conflicts of interest

There are no conflicts to declare.

Acknowledgements

D. R. T. Zahn and O. Raievska acknowledge financial support by the Deutsche Forschungsgemeinschaft (DFG project ZA-146/45-1).

Notes and references

1 L. Jing, S. V. Kershaw, Y. Li, X. Huang, Y. LI, A. L. Rogach and M. Gao, *Chem. Rev.*, 2016, **116**, 10623.
2 O. Stroyuk, A. Raevskaya and N. Gaponik, *Chem. Soc. Rev.*, 2018, **47**, 5354.
3 A. E. Raevskaya, M. V. Ivanchenko, O. L. Stroyuk, S. Ya. Kuchmiy and V. F. Plyusnin, *J. Nanopart. Res.*, 2015, **17**, 135.
4 A. Raevskaya, V. Lesnyak, D. Haubold, V. Dzhagan, O. Stroyuk, N. Gaponik, D. R. T. Zahn and A. Eychmüller, *J. Phys. Chem. C*, 2017, **121**, 9032.
5 A. Raevskaya, O. Rosovik, A. Kozytskiy, O. Stroyuk, V. Dzhagan and D. R. T. Zahn, *RSC Adv.*, 2016, **6**, 100145.
6 A. Raevskaya, O. Rozovik, A. Novikova, O. Selyshchev, O. Stroyuk, V. Dzhagan, I. Goryacheva, N. Gaponik, D. R. T. Zahn and A. Eychmüller, *RSC Adv.*, 2018, **8**, 7550.

7 O. Stroyuk, A. Raevskaya, F. Spranger, O. Selyshchev, V. Dzhagan, S. Schulze, D. R. T. Zahn and A. Eychmüller, *J. Phys. Chem. C*, 2018, **122**, 13648.
8 O. Stroyuk, F. Weigert, A. Raevskaya, F. Spranger, C. Würth, U. Resch-Genger, N. Gaponik and D. R. T. Zahn, *J. Phys. Chem. C*, 2019, **123**, 2632.
9 O. Raievska, O. Stroyuk, Y. Azhniuk, D. Solonenko, A. Barabash, C. J. Brabec and D. R. T. Zahn, *J. Phys. Chem. C*, 2020, **124**, 19375.
10 A. E. Raevskaya, M. V. Ivanchenko, M. A. Skoryk and O. Stroyuk, *J. Lumin.*, 2016, **178**, 295.
11 O. Stroyuk, A. Raevskaya, F. Spranger, N. Gaponik and D. R. T. Zahn, *ChemPhysChem*, 2019, **20**, 1640.
12 O. Stroyuk, V. Dzhagan, A. Raevskaya, F. Spranger, N. Gaponik and D. R. T. Zahn, *J. Lumin.*, 2019, **215**, 116630.
13 M. S. Bootharaju, W. Baek, S. Lee, H. Chang, J. Kim and T. Hyeon, *Small*, 2020, 2002067.
14 C. Palencia, K. Yu and K. Boldt, *ACS Nano*, 2020, **14**, 1227.
15 Y. Kimura, Y. Saito, T. Nakada and C. Kaito, *Phys. E*, 2002, **13**, 11.
16 H. Mori, H. Yasuda and K. Fujii, *Surf. Rev. Lett.*, 1996, **3**, 1177.
17 M. Tsuji, C. Shiraishi, M. Hattori, A. Yajima, M. Mitarai, K. Uto, K. Takemura and Y. Nakashima, *Chem. Commun.*, 2013, **49**, 10941.
18 T. Shibata, B. A. Bunker, Z. Zhang, D. Meisel, C. F. Vardeman II and J. D. Gezelter, *J. Am. Chem. Soc.*, 2002, **124**, 11989.
19 E. Ma, H. W. Sheng, J. H. He and P. J. Shilling, *Mater. Sci. Eng., A*, 2000, **286**, 48.
20 Y. Shimizu, K. S. Ikeda and S. Sawada, *Phys. Rev. B*, 2001, **64**, 075412.
21 Y. Shimizu, S. Sawada and K. S. Ikeda, *Eur. Phys. J. D*, 1998, **4**, 365.
22 H. Mori and H. Yasuda, *Bull. Mater. Sci.*, 1999, **22**, 181.
23 H. Yasuda and H. Mori, *Intermetallics*, 1996, **4**, S225.
24 K. R. Krishnadas, A. Baksi, A. Ghosh, G. Natarajan and T. Pradeep, *Nat. Commun.*, 2016, **7**, 13447.